Influence of the Southern Annular Mode on the sea ice–ocean system

W. Lefebvre and H. Goosse
Université Catholique de Louvain, Institut d'Astronomie et de Géophysique Georges Lemaître, Belgium

R. Timmermann
Alfred Wegener Institute for Polar and Marine Research, Bremerhaven, Germany

T. Fichefet
Université Catholique de Louvain, Institut d'Astronomie et de Géophysique Georges Lemaître, Louvain-la-Neuve, Belgium

Received 30 March 2004; revised 25 May 2004; accepted 7 July 2004; published 16 September 2004.

[1] The global sea ice–ocean model ORCA2-LIM, driven by the NCEP/NCAR (National Centers for Environmental Prediction-National Center for Atmospheric Research) reanalysis daily 2-m air temperatures and 10-m winds and by monthly climatologies for precipitation, cloud cover, and relative humidity, is used to investigate the impact of the Southern Annular Mode (SAM) on the Antarctic sea ice-ocean system. Our results suggest that the response of the circumpolar Southern Ocean consists of an annular and a non-annular component. For the sea ice cover, the non-annular component seems to be the most important. The annular component strongly affects the overall patterns of the upper ocean circulation. When the SAM is in its positive phase, a northward surface Ekman drift, a downwelling at about 45°S, and an upwelling in the vicinity of the Antarctic continent are simulated. The non-annular component has a significant impact at the regional scale, especially in the Weddell, Ross, Amundsen, and Bellingshausen Seas. In those regions, the pressure pattern associated with the SAM induces meridional winds which advect warmer air in the Weddell Sea and around the Antarctic Peninsula and colder air in the Amundsen and Ross Seas. This implies a dipole response of sea ice to the SAM, with on average a decrease in ice area in the Weddell Sea and around the Antarctic Peninsula and an increase in the Ross and Amundsen Seas during years with a high SAM index. The long-term trend in the observed sea ice area does not appear to be related to the trend in the SAM index. *INDEX TERMS:* 4215 Oceanography: General: Climate and interannual variability (3309); 4207 Oceanography: General: Arctic and Antarctic oceanography; 1863 Hydrology: Snow and ice (1827); 3339 Meteorology and Atmospheric Dynamics: Ocean/atmosphere interactions (0312, 4504); *KEYWORDS:* SAM, Antarctic, sea ice–ocean system

Citation: Lefebvre, W., H. Goosse, R. Timmermann, and T. Fichefet (2004), Influence of the Southern Annular Mode on the sea ice–ocean system, *J. Geophys. Res.*, *109*, C09005, doi:10.1029/2004JC002403.

1. Introduction

[2] The circulation variability of the lower atmosphere in the Southern Hemisphere is dominated by an annular mode that significantly influences the strength of the westerlies [e.g., *Connolley*, 1997; *Gong and Wang*, 1999; *Thompson and Wallace*, 2000; *Simmonds*, 2003]. This mode has been referred to as the High Latitude Mode (HLM), the Antarctic Oscillation (AAO), or the Southern Annular Mode (SAM). We will use the latter name and follow *Thompson and Wallace* [2000] in defining the SAM as the leading principal component (PC) of the 850-hPa geopotential height anomalies south of 20°S (or of the sea level pressure; the corresponding time series displaying a correlation of 0.99). The index time series can be found at http://www.jisao.washington.edu/aao/slp/. A positive (negative) SAM index is associated with lower (higher) sea level pressures at high latitudes and higher (lower) sea level pressures at low latitudes (Figure 1). As a consequence, during years with a positive SAM index, the westerlies are intensified in the region of the Antarctic Circumpolar Current (ACC) and weakened north of 40°S. These characteristics are not confined to the lower levels of the atmosphere since the variability of the circulation at 500 hPa, 300 hPa, and in the stratosphere is also dominated by an annular mode [e.g., *Kidson*, 1999; *Thompson and Wallace*, 2000; *Mo*, 2000; *Genthon et al.*, 2003]. Although the variability associated with SAM has a mostly zonal structure, a non-annular component can be found in the NCEP-NCAR and ECMWF reanalyses as well as in coupled model simulations [e.g., *Mo*, 2000; *Limpasuvan and Hartmann*, 2000; *Cai and Watterson*, 2002; *Hall and Visbeck*, 2002; *Genthon et al.*, 2003]. In particular, a low pressure anomaly west of the

Copyright 2004 by the American Geophysical Union.
0148-0227/04/2004JC002403

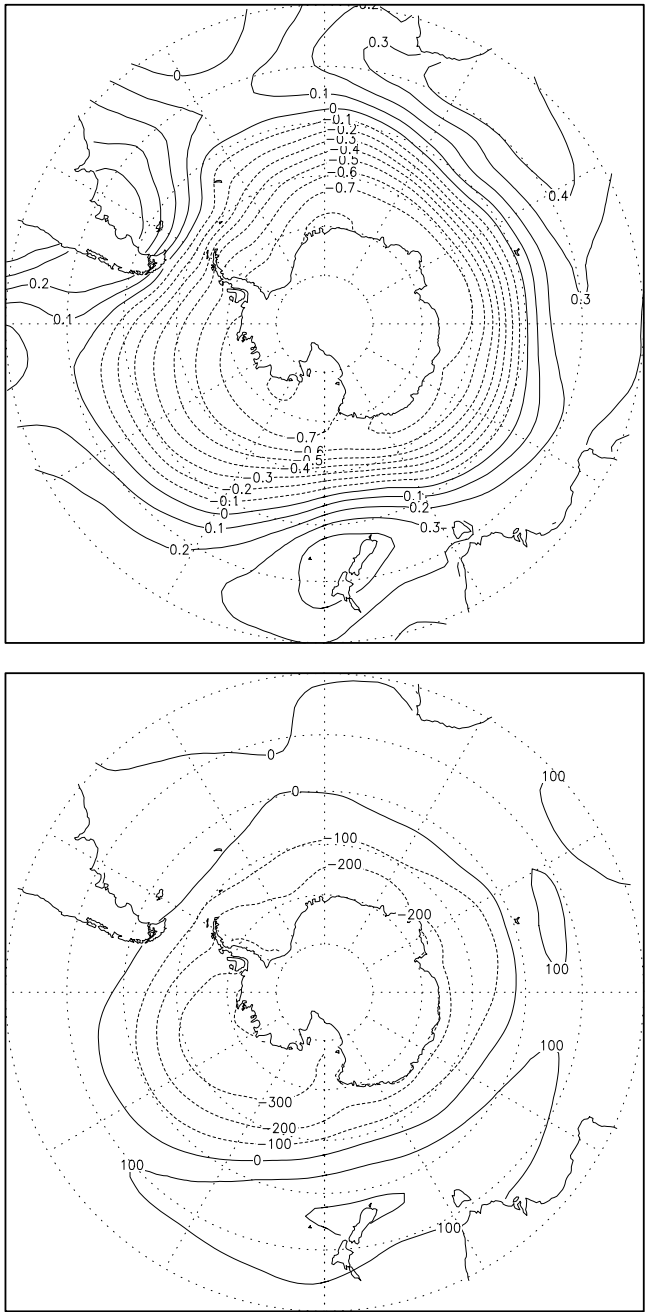

Figure 1. (top) Annually averaged correlation between the seasonal mean (JFM, AMJ, JAS, OND) atmospheric surface pressure (NCEP-NCAR) and the seasonal mean SAM index for the period 1960–1999. (bottom) Annually averaged regression (Pa) between the seasonal mean atmospheric surface pressure and the seasonal mean SAM index.

Antarctic Peninsula is found for high values of the SAM index (Figure 1).

[3] In a recent study, *Thompson and Solomon* [2002] have suggested that a high SAM index favors cooling over Antarctica, due to an increased isolation of the Antarctic continent. An important exception is the Antarctic Peninsula, where the enhanced westerlies associated with a high SAM index increase the advection of relatively warm oceanic air resulting in a significant warming of the area.

[4] Atmospheric variability associated with SAM has an significant impact on the sea ice cover and the oceanic circulation. Because of the lack of observations, this effect has been mainly studied with Climate General Circulation Models (CGCMs) [e.g., *Watterson*, 2000, 2001; *Cai and Watterson*, 2002; *Hall and Visbeck*, 2002]. As those models are able to reproduce the observed characteristics of the SAM in the atmosphere reasonably well, a realistic response of the ocean and of the sea ice pack to the SAM can be expected. In particular, *Hall and Visbeck* [2002] summarized the influence of SAM in their model as follows. Stronger westerlies in the region of the ACC induce an intensified eastward surface ocean current and, as a result of the Ekman drift, a stronger northward surface current south of 45°S. North of 45°S, the pattern is reversed due to weaker westerlies. This causes an upwelling in the ocean around 65°S and a downwelling around 45°S. Positive phases of SAM are also associated with an oceanic heat divergence at about 60°S and a heat convergence at about 40°S, leading to a modest decrease in sea surface temperature (SST) at high latitudes and a weak cooling at midlatitudes. In addition to the role of wind stress variations discussed above, *Watterson* [2000] showed that surface heat fluxes are very important in generating anomalies of SST.

[5] In the model of *Hall and Visbeck* [2002], the sea ice velocity is set equal to the velocity of the first oceanic level. As a consequence, because of the stronger northward oceanic current south of 45°S, model ice is driven northward when the SAM index is positive. This yields a decrease in ice thickness close to the Antarctic continent, an increase farther north, and a more extensive ice cover. However, using satellite observations, *Kwok and Comiso* [2002] and *Liu et al.* [2004] showed that the response of the sea ice to SAM variability over the last 20 years is different from the one proposed by *Hall and Visbeck*, 2002 as it appears to be mainly characterized by a decrease in the Weddell and Bellingshausen sectors and an increase in the Ross and Amundsen sectors, i.e., by a non-annular response. On the basis of the SSMR/SSMI satellite data, *Liu et al.* [2004] also showed that the recent trends in the sea ice area cannot be attributed to SAM nor to the El Niño Southern Oscillation (ENSO).

[6] The goal of the present study is to provide further information on the response of the ice-ocean system to the variability associated with SAM. The study is based on a numerical experiment performed with the coupled sea ice-ocean model ORCA2-LIM [*Timmermann et al.*, 2005, 2004]. Similar simulations with different models have been carried out to investigate the variability of the sea ice cover and of deep water formation in the Southern Ocean [e.g., *Beckmann and Timmermann*, 2001; *Timmermann et al.*, 2002a, 2002b; *Fichefet et al.*, 2003a, 2003b]. Nevertheless, in contrast to the Northern Hemisphere where such a type of analysis is common and fruitful [e.g., *Proshutinsky and Johnson*, 1997; *Zhang et al.*, 2000; *Krahmann and Visbeck*, 2003], those experiments have not been used to systematically investigate the influence of a particular atmospheric mode of variability on sea ice and ocean. We will take profit of the complementarity of the approach proposed here to the previous studies conducted with CGCMs. On the one hand, CGCMs provide consistent fields from the top of the atmosphere to the bottom of the

ocean. On the other hand, we employ a relatively sophisticated ice-ocean model with a higher resolution and more complete physics than in the CGCM studies. Furthermore, the use of atmospheric reanalysis data avoids possible model biases resulting in a better representation of the Southern Ocean in ice-ocean models than in CGCMs.

[7] The model and the forcing are briefly described in section 2. Section 3 presents the response of the model to the SAM in the zonal mean and compares our results to the previous investigations. This is followed by a discussion of the non-zonal component of the response, which appears quite important in our model and has not been thoroughly analyzed before with an OGCM. Conclusions are presented in section 4.

2. Model Description and Experimental Design

[8] The model used here, called ORCA2-LIM, results from the coupling of the Louvain-la-Neuve sea ice model (LIM) [*Fichefet and Morales Maqueda*,1997] with the hydrostatic, primitive equation ocean model OPA (Océan PArallélisé) [*Madec et al.*, 1999]. OPA is a finite difference ocean general circulation model with a free surface and a nonlinear equation of state in the *Jackett and McDougall* [1995] formulation. In the ORCA2-LIM configuration, lateral tracer mixing is done along isopycnals. Eddy-induced tracer advection is parameterized following *Gent and McWilliams* [1990] with the coefficients decreased between 20°N and 20°S. Momentum is mixed along model level surfaces using coefficients varying with latitude, longitude, and depth. Vertical eddy diffusivity and viscosity coefficients are computed from a level-1.5 turbulence closure scheme based on a prognostic equation for the turbulent kinetic energy [*Blanke and Delecluse*, 1993]. Double diffusive mixing (i.e., salt fingering and diffusive layering) is computed following *Merryfield et al.* [1999]. In locations with a statically unstable stratification, a value of 100 $m^2\ s^{-1}$ is assigned to the vertical eddy coefficients for momentum and tracers. The *Beckmann and Döscher* [1997] bottom boundary layer scheme ensures an improved representation of dense water spreading over topography in this geopotential-coordinate model.

[9] The thermodynamic part of LIM uses a three-layer model (one layer for snow and two layers for ice) for sensible heat storage and vertical heat conduction within snow and ice. Vertical and lateral sea ice growth/decay rates are obtained from energy budgets at the upper and lower surfaces of the snow-ice cover, and at the surface of leads present within the ice pack. At the upper surface, a prognostic treatment of the temperature in a very thin surface layer is used. The effect of the subgrid-scale snow and ice thickness distributions is accounted for through an effective thermal conductivity, which is computed by assuming that the snow and ice thicknesses are uniformly distributed between zero and twice their mean value over the ice-covered portion of the grid cell. Storage of latent heat inside the ice resulting from the trapping of shortwave radiation by brine pockets is taken into account. When the load of snow is large enough to depress the snow-ice interface under the water level, seawater is assumed to infiltrate the entirety of the submerged snow and to freeze there, forming a snow ice cap. The ice concentration, the snow volume per unit area, the ice volume per unit area, the snow enthalpy per unit area, the ice enthalpy per unit area, and the brine reservoir per unit area are advected with the ice drift velocity.

[10] The sea ice velocity field is determined from a momentum balance considering sea ice as a two-dimensional continuum in dynamical interaction with atmosphere and ocean. The viscous-plastic constitutive law proposed by *Hibler* [1979] is used for computing internal stress within the ice for different states of deformation. The model also includes a parameterization for the formation of leads due to shearing deformation following *Stern et al.* [1995].

[11] The coupled model is run on a global grid with 2° nominal resolution and a mesh refinement in high latitudes and near the equator. As a consequence, the meridional resolution increases to 0.5° close to the Antarctic continent, corresponding to a horizontal grid width of ~50 km. Vertical discretization uses 30 z-levels, with 10 levels in the top 100 m. Model runs are initialized using data from the end of the 46-year experiment described by *Timmermann et al.* [2005].

[12] Daily 2-m air temperatures and 10-m winds from the NCEP/NCAR reanalysis project for the period 1948–1999 [*Kalnay et al.*, 1996], and monthly climatologies of surface relative humidity [*Trenberth et al.*, 1989], cloud fraction [*Berliand and Strokina*, 1980], and precipitation rate [*Xie and Arkin*, 1996] are utilized to drive the model. The surface fluxes of heat and moisture are determined from these data by using empirical parameterizations described by *Goosse* [1997]. Evaporation/sublimation is derived from the turbulent flux of latent heat. In addition, a correction of ocean surface freshwater fluxes has been derived from the time-mean restoring salinity flux diagnosed from the experiment described by *Timmermann et al.* [2005] in order to circumvent the surface salinity drift that occurs through the lack of any stabilizing feedback if the model is forced with slightly incorrect evaporation, precipitation, and/or river runoff fields. The momentum fluxes at the various interfaces are obtained from standard bulk formulas. The parameterization of *Large and Pond* [1981] is utilized to compute the drag coefficient between air and water. For the drag coefficients between air and snow/ice and between ice and water, we use constant values of 2.25×10^{-3} and 5×10^{-3}, respectively. This leads to a ratio of these two coefficients of 0.45, which is consistent with values adopted in other modeling studies of the Antarctic sea ice [e.g., *Stössel*, 1992; *Fischer and Lemke*, 1994; *Harder and Fischer*, 1999]. Further details of the coupled model are given by *Timmermann et al.* [2005, 2004].

[13] The quality of the NCEP-NCAR data set is questionable in polar regions because of the small number of observations there, in particular for the period prior to the start of the assimilation of satellite data in the late 1970s [e.g., *Hines et al.*, 2000; *Marshall*, 2002; *Struraro*, 2003]. As a consequence, the analysis presented here will be performed on the last 20 years of the experiment. Even during this period, some uncertainties remain. An attempt to use the cloud cover, precipitation, and humidity from the NCEP-NCAR reanalysis data induced large errors in polar regions [*Timmermann et al.*, 2005], which forced us to use climatologies for these variables. This implies that interannual variability of latent and solar heat fluxes and of the precipitation rate is not properly taken into account in our

simulations. However, *Timmermann et al.* [2005] have shown that this forcing strategy still yields a good representation of the interannual variability of the sea ice cover. Furthermore, the conclusions derived from model results are compared to available observations (see end of section 3) to estimate, at least qualitatively, the impact of these shortcomings.

3. Results

3.1. Zonal Mean Response

[14] For zonal mean fields, the SAM index is highly correlated with the zonal and meridional wind stresses as well as with the zonal, meridional and vertical currents simulated by the model, with peak correlations between 0.6 and 0.8 (Figure 2). This suggests that a substantial part of the large-scale current variability in the Southern Ocean is due to the SAM. The strong positive correlation with the zonal wind stress between 45°S and 65°S (Figure 2, top) is straightforward from the pressure pattern associated with the SAM (Figure 1), while the negative correlation with the meridional wind stress in the same latitude band mainly arises from the rotation of the wind vector in the surface boundary layer. The stronger westerlies found for positive SAM index induce enhanced zonal ocean surface currents and, due to the Ekman drift, also stronger meridional currents (Figure 2, middle). This results in a horizontal divergence at about 65°S, near the Antarctic continent, which leads to oceanic upwelling there. Besides, a horizontal convergence is found at about 45°S and, consequently, downwelling occurs there. The northward transport in the upper ocean is balanced by a southward return flow below 1500 m (Figure 2, middle). This indicates that the SAM has a large influence on the ocean currents over the whole water column as also shown by the correlation with vertical motion, which remains high even in the deep ocean (Figure 2, bottom).

[15] The correlation between the simulated zonal mean mixed layer depth with the SAM index has a broad peak between 40°S and 65°S, with a maximum value exceeding 0.6 (Figure 3). This corresponds to a regression between the SAM index and the mixed layer depth of 5 to 7 m in summer and up to 50 m in winter. Since the latitudinal band 40°S–65°S is also the region with the maximum increase in the magnitude of the wind stress, the deeper mixed layers are likely due to a higher wind stirring of the water column. Variations of the density flux at the ocean surface are only weakly correlated with the simulated mixed layer depths. The density flux in our simulation even tends to stabilize the water column at latitudes with an increased mixed layer depth, which shows that the effect of the density flux on the simulated mixed layer depth is negligible. However, we must recall here that the forcing used in our simulation does not include any interannual variation in precipitation and features only a reduced variability of surface heat fluxes. Taking into account this additional variability might alter

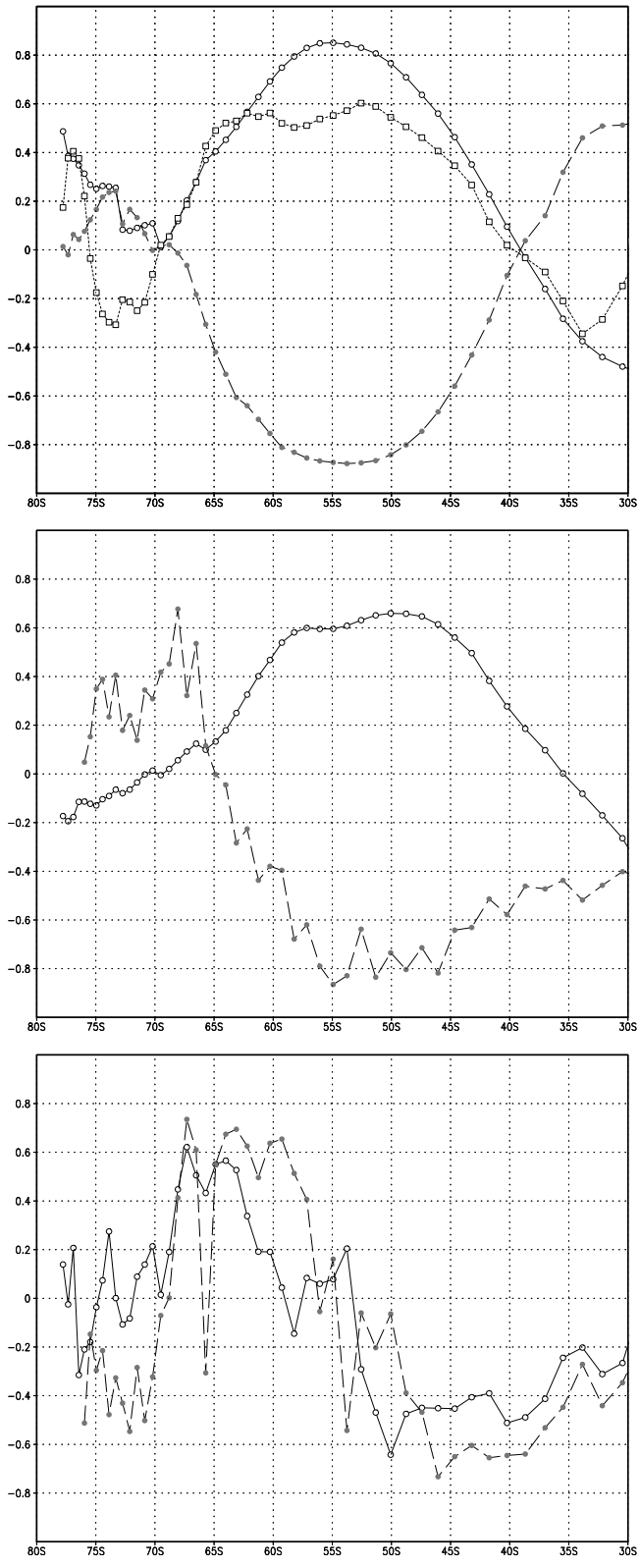

Figure 2. Correlation between the annual means of the SAM index and (top) the zonal means of the zonal wind stress (solid line with open circles), the meridional wind stress (long dashed line with circles), and the zonal current at the surface (dotted line with squares), (middle) the meridional current at the surface (solid line with circles) and at 2290 m depth (long dashed line with circles), and (bottom) the vertical current at 45 m depth (solid line with circles) and at 2290 m depth (long dashed line with circles).

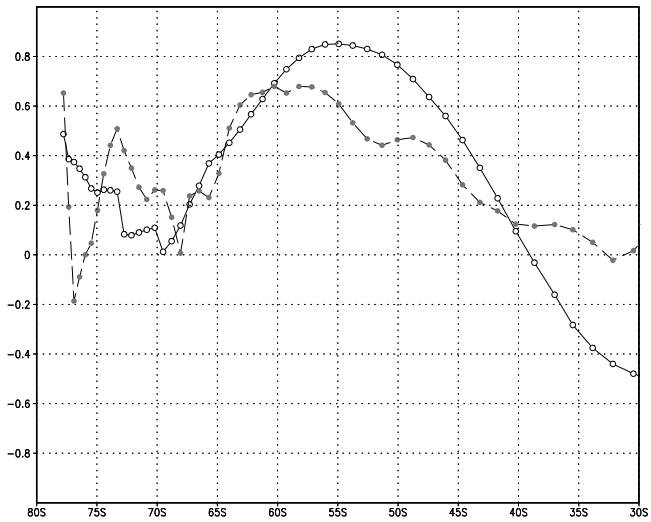

Figure 3. Correlation between the annual mean SAM index and the annual mean zonally averaged zonal wind stress (solid line with open circles), and the mixed layer depth (long dashed line with circles).

the conclusion about the effect of the SAM on the density flux [e.g., *Genthon et al.*, 2003].

[16] We can consider all correlations above 0.4 as significant with a confidence of more than 95%. All the SAM-related changes in the ocean currents (Figure 2) and also the increased mixed layer depth (Figure 3) between 65°S and 45°S are therefore significant. In contrast to that, Figure 4 (top) shows that the SAM explains only a very small fraction of the variations of the zonal mean surface air temperature over the ocean and of the modeled sea surface temperature (SST) in our simulation. The correlation between the SAM and the atmospheric temperature is smaller than 0.1 at all latitudes and thus not significant. The correlation with the SST has a slightly higher magnitude, but it barely exceeds −0.2 between 55°S and 65°S. This result is in qualitative agreement with the one obtained by *Hall and Visbeck* [2002], but the magnitude of the response is smaller here. Southward of 65°S, a complex pattern is found with cooling between 70°S and 74°S and warming in the latitudinal bands 68°S–70°S and 74°S–77°S, a feature not present in the *Hall and Visbeck* [2002] study. This results from different responses in the various sectors of the Southern Ocean as discussed in the next section. At depth, the temperature in the Southern Ocean tends to decrease when the SAM index is positive and to do so over the whole range of latitudes (south of 50°S). This can be explained by the intensified overturning (Figure 2) that brings cold deep water upward.

[17] The correlation between the SAM index and the ice thickness is higher than the one with SST, but it still has a modest magnitude (Figure 4, middle) and is only marginally

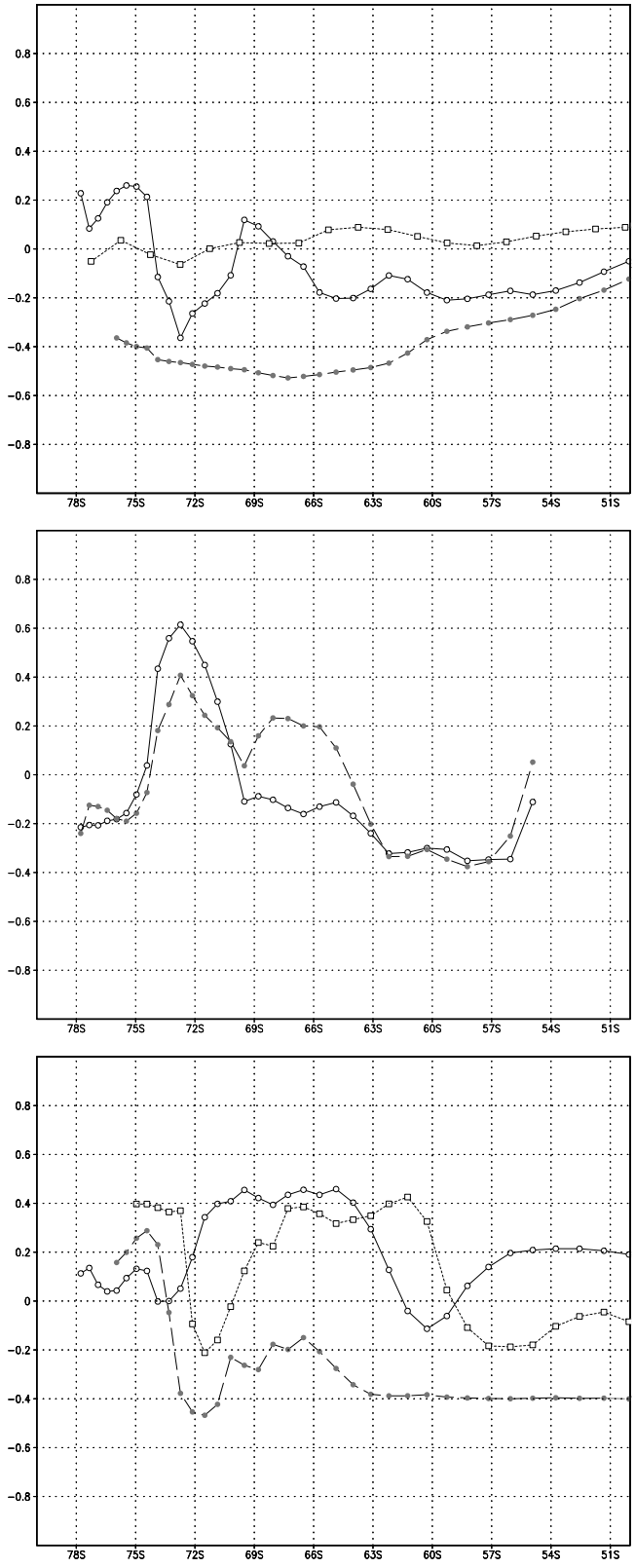

Figure 4. Correlation between the annual mean SAM index and the annual mean zonally averaged (top) 2-m air temperature over the ocean (NCEP-NCAR) (dotted line with squares), sea surface temperature (solid line with open circles), and ocean temperature at 2290 m depth (long dashed line with circles), (middle) ice thickness (solid line with open circles) and ice concentration (long dashed line with circles), and (bottom) sea surface salinity (solid line with open circles), salinity at 2290 m depth (long dashed line with circles), and salinity at 3752 m depth (dotted line with squares).

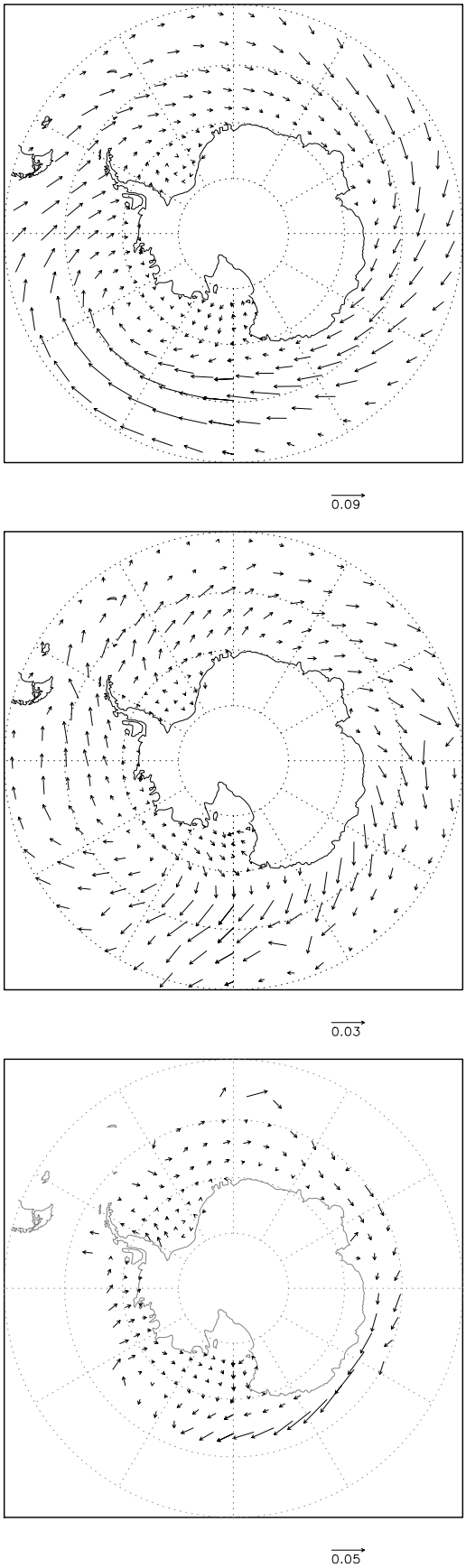

significant. Northward of 70°S, a negative correlation is found with a maximum value of about −0.4, and a positive correlation is found southward of this latitude with a peak value of 0.6. The correlation with the ice concentration features a similar pattern. These results are in contrast to the ones of *Hall and Visbeck* [2002], who found negative correlations with the ice thickness close to the coast and positive ones offshore. This difference is due to the different techniques used to compute the ice velocity in the two models. *Hall and Visbeck* [2002] assume that the ice is transported at the surface velocity of the ocean. This velocity has a strong diverging component resulting in a decrease in ice thickness close to the coast and a larger extension of the pack when the SAM index is positive. In our model, the response of the ocean surface velocity is similar to the one described by *Hall and Visbeck* [2002] (Figure 5, middle). Nevertheless, when solving the full momentum balance for sea ice, the angle between the wind stress and the ice velocity is much smaller than between the wind stress and the ocean velocity. *Thorndike and Colony* [1982] and *Hibler* [1986] estimated that this angle is of the order of 20°. As a consequence, the divergence of the ice is much weaker than the one of the ocean at surface and the regression between ice velocity and the SAM index provides mainly a zonal transport that only has a little effect on the ice distribution. Hence the correlation between the zonal mean meridional sea ice velocity and the SAM index is always smaller than 0.3 in absolute value. The details of the sea ice response in our model will be discussed in section 3.2.

[18] Finally, the results of our model simulation allow studying the impact of the SAM on the salinity distribution in the ocean (Figure 4, bottom). In the zonal mean, we can easily explain the salinity variations by looking at the ocean current anomalies. The enhanced overturning and the increased northward currents cause a rise in sea surface salinity (SSS). At depth (around 2000 m) the increased southward currents are responsible for a decrease in salinity. Owing to the inflow of saltier water from the Atlantic Ocean, the salinity around 3700 m rises again with increasing SAM south of 60°S. However, the magnitude of variability strongly decreases with depth: Variations of the zonal mean SSS exceed 0.1 psu, while salinity signals in the deep ocean are about 0.01 psu at 2290 m, and only 0.001 psu at 3700 m depth.

[19] All results discussed above have been obtained with a zero time lag, since this has been found to yield the maximum correlations between the SAM index and the ocean currents. However, the correlation between SAM and

Figure 5. (top) Annual mean of the regression of the horizontal wind stress (N/m^2) with the annual mean SAM index for the period 1980–1999. (middle) Annual mean of the regression of horizontal ocean surface currents (m/s) with the annual mean SAM index for the period 1980–1999. (Bottom) Winter (July, August, September) regression of the ice velocity (m/s) with the seasonal mean SAM index for the period 1980–1999. Only points in which the ice concentration is higher than 0.15 for at least 10 years are taken into account. For clarity, only one sixteenth of the vectors are shown.

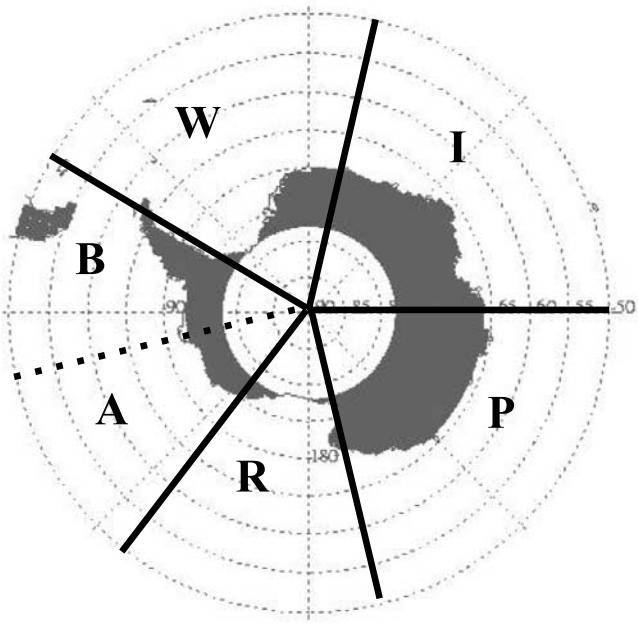

Figure 6. Sectors of the Southern Ocean used for analysis of results. These are the Weddell Sea (W; 60°W–20°E), the Indian Ocean (I; 20°E–90°E), the Pacific Ocean (P; 90°E–160°E), the Ross Sea (R; 160°E–140°W), and the Amundsen-Bellingshausen Seas (AB; 140°W–60°W).

the oceanic temperature increases by about 10% for a time lag of 4 months, with the SAM index leading, due to the huge heat capacity of water. Since this increase appears rather small and does not affect our conclusions, all further analysis continues using a zero time lag.

3.2. Geographical Response

[20] The results discussed in the previous section have revealed that the SAM explains only a small fraction of the variability of the simulated zonal mean SST, ice thickness, and ice concentration. This leads to two contrasting hypotheses. The first one is that the SAM is very useful for understanding the oceanic current structure but not for understanding the SST and ice cover patterns. The second one assumes that the SAM has an influence on the SST and the ice cover in various regions but, as this impact may have a different sign at different longitudes along one latitudinal band, it is not seen clearly in the zonal mean. The goal of this section is to decide which of these two hypotheses is valid.

[21] As mentioned in sections 1 and 3.1, the correlation between the SAM index and the atmospheric surface pressure (Figure 1) has a clear annular component. Nevertheless, this pressure pattern is not perfectly annular. Specifically, a low pressure anomaly is found in the Amundsen and Ross sectors when the SAM index is high (the division in sectors can be seen in Figure 6). This yields a significant meridional component of the surface wind stress in these regions (Figure 5, top), which is directed toward the south in the Weddell, Amundsen, and Bellingshausen Seas and toward the north in the Ross Sea. A similar pattern can be found in the ECMWF (European Centre for Medium-range Weather Forecasts) reanalysis data and also in results from CGCMs [e.g., *Hall and Visbeck*, 2002; *Mo*, 2000; *Limpasuvan and Hartmann*, 2000; *Cai and Watterson*, 2002; *Genthon et al.*, 2003].

[22] In the zonal mean, the anomalies of ocean surface currents are eastward and northward south of 45°S for a high SAM index (Figures 2 and 5, middle), but the non-annular component of the pressure pattern associated with the SAM has a clear local impact. In the Bellingshausen Sea, the correlation between the SAM index and the meridional surface currents is only slightly positive, with a very small divergence of the surface currents and a weak upwelling there. In the Ross Sea, currents associated with a high SAM index are westward close to the coast and have a very strong northward component offshore. Sector by sector, there do not seem to be huge differences between the various regions (Table 1). Nevertheless, in the Amundsen-Bellingshausen Seas, high values of the SAM index are correlated with an intensified upwelling in the western sector that compensates for the very small vertical motion in the eastern Bellingshausen Sea. In the Ross Sea, there is a slightly more pronounced Ekman pumping due to the southerly winds in that region.

[23] Although the meridional component of the wind associated with the SAM has a much weaker magnitude than the zonal one, it can have a significant influence on the atmospheric temperature because of the meridional atmospheric temperature gradient. In particular, the southward transport in the vicinity of the Antarctic Peninsula is likely to play a role in the warming observed there during years with positive SAM index. This explanation is complementary to the hypothesis of *Thompson and Solomon* [2002] that attributes the local warming for a positive SAM index to an increase in the zonal flow. The increase in the southward component of near-surface winds (Figure 5) could also explain the air temperature rise at Orcada station (61°S, 45°W) that was not discussed by *Thompson and Wallace* [2000]. Furthermore, a strong temperature signal in the NCEP-NCAR reanalysis is found in the eastern Ross Sea, the Amundsen Sea, and the western Bellingshausen Sea, which is consistent with a response of the temperature to the anomalous meridional transport in those areas. Unfortunately, the temperature changes in this area were not analyzed by *Thompson and Solomon* [2002] because of the lack of station data in those regions.

Table 1. Correlation of the SAM Index With the Vertical Current Anomaly at 45 m Depth (W), the Sea Surface Salinity (SSS) Anomaly, the Sea Surface Temperature (SST) Anomaly, and the Ice Covered Area Anomaly (Ice Concentration >15%) for the Period 1980–1999 for all Seasons[a]

	Weddell	Indian	Pacific	Ross	Amundsen-Bellingshausen
W(M)	0.50[c]	0.56[c]	0.50[c]	0.67[c]	0.46[c]
SSS(M)	0.35[b]	0.46[c]	0.39[c]	0.23	0.23
SST (M)	0.45[c]	−0.10	−0.25	−0.69[c]	−0.17
Ice area (M)	−0.29[c]	−0.16	0.05	0.27[c]	0.18
Ice area (O)	−0.30[c]	0.33[c]	0.25[b]	0.20	−0.02

[a]For the vertical currents, the SST and the SSS, only the region south of 55°S is taken into account. M: Model results. O: Observations according to the HadISST data set [*Rayner et al.*, 2003]. Each time series consists of 80 values. The significance has been tested using a Monte-Carlo method with 1,000,000 simulations of autocorrelated data series with the same autocorrelation as the time series presented in the table.
[b]Correlations exceeding the 90% significance thresholds.
[c]Correlations of more than 95% significance.

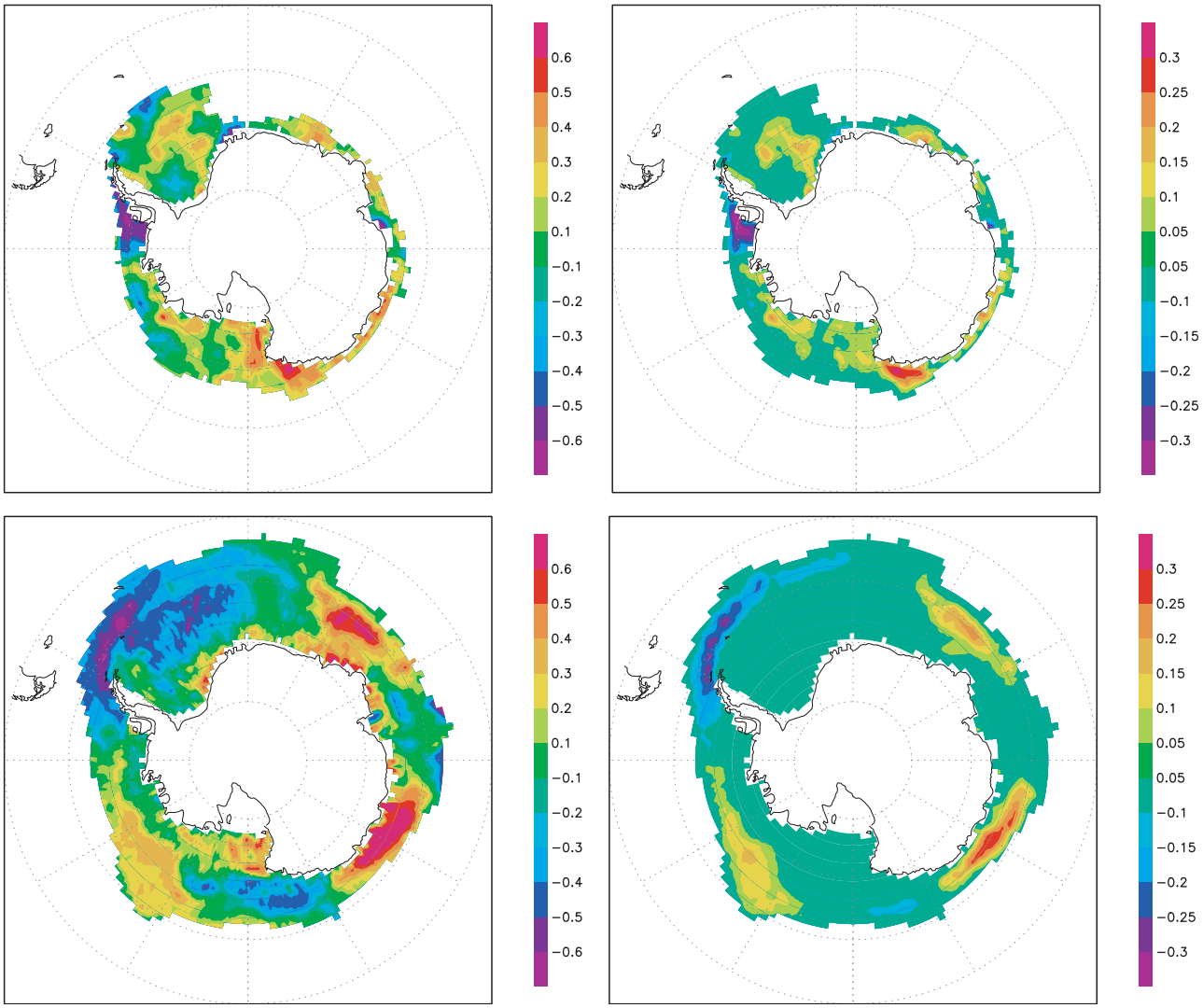

Figure 7. (left) Correlation and (right) regression between the seasonal mean SAM index and the seasonal mean ice concentration for the period 1980–1999 in the HadISST1 observations [*Rayner et al.*, 2003]. (top) January, February, and March. (bottom) July, August, and September.

[24] The non-annular component of the wind pattern associated with the SAM also affects the SST through its influence on oceanic currents and on air temperature. In general, there is a cooling in all sectors during years with a high SAM index, which is consistent with the zonal mean response (see Figure 4). Nevertheless, because of the strong northward wind associated with a high SAM index in the Ross Sea, the cooling is much larger there (Table 1). The SST in the Weddell Sea, in turn, rises when the SAM index is positive, due to the enhanced advection of warm air and stronger oceanic upwelling that brings warmer water to the surface. In the Pacific and Indian sectors, the response is less clear. Northward of 60°S, the SST decreases as expected but, during some seasons, it increases close to the continent because of the large increase in upwelling there. When averaged over the Amundsen-Bellingshausen sector, only a small response remains. This is the result of a warming on the eastern part of this sector because of a stronger advection of warm air here and a cooling in the western part due to southerly winds there. In contrast to the SST, surface salinity changes do not show large differences between the various regions and the response is well represented by the zonal mean as discussed in section 3.1 (see also Table 1 and Figure 4, bottom).

[25] The response of the simulated ice concentration generally follows the wind anomaly pattern and the changes in SST, with a general increase in the Ross Sea and a decrease in the Weddell Sea for positive phases of the SAM (Table 1). When analyzing the regional patterns season by season, the correspondence between the observations (Figure 7) and the model (Figure 8) remains quite good. In particular, both model and data feature a large decrease of ice coverage in the Weddell Sea and an increase in the Ross Sea in winter during years with a high SAM index. Likewise, following the anomalies of near-surface winds (Figure 5, top) and ice drift (Figure 5, bottom), the Amundsen-Bellingshausen sector features a decrease of ice area around the Antarctic Peninsula and an increase in the Amundsen Sea during years with a high SAM index. This is in close agreement with the results of *Liu et al.* [2004] and *Kwok*

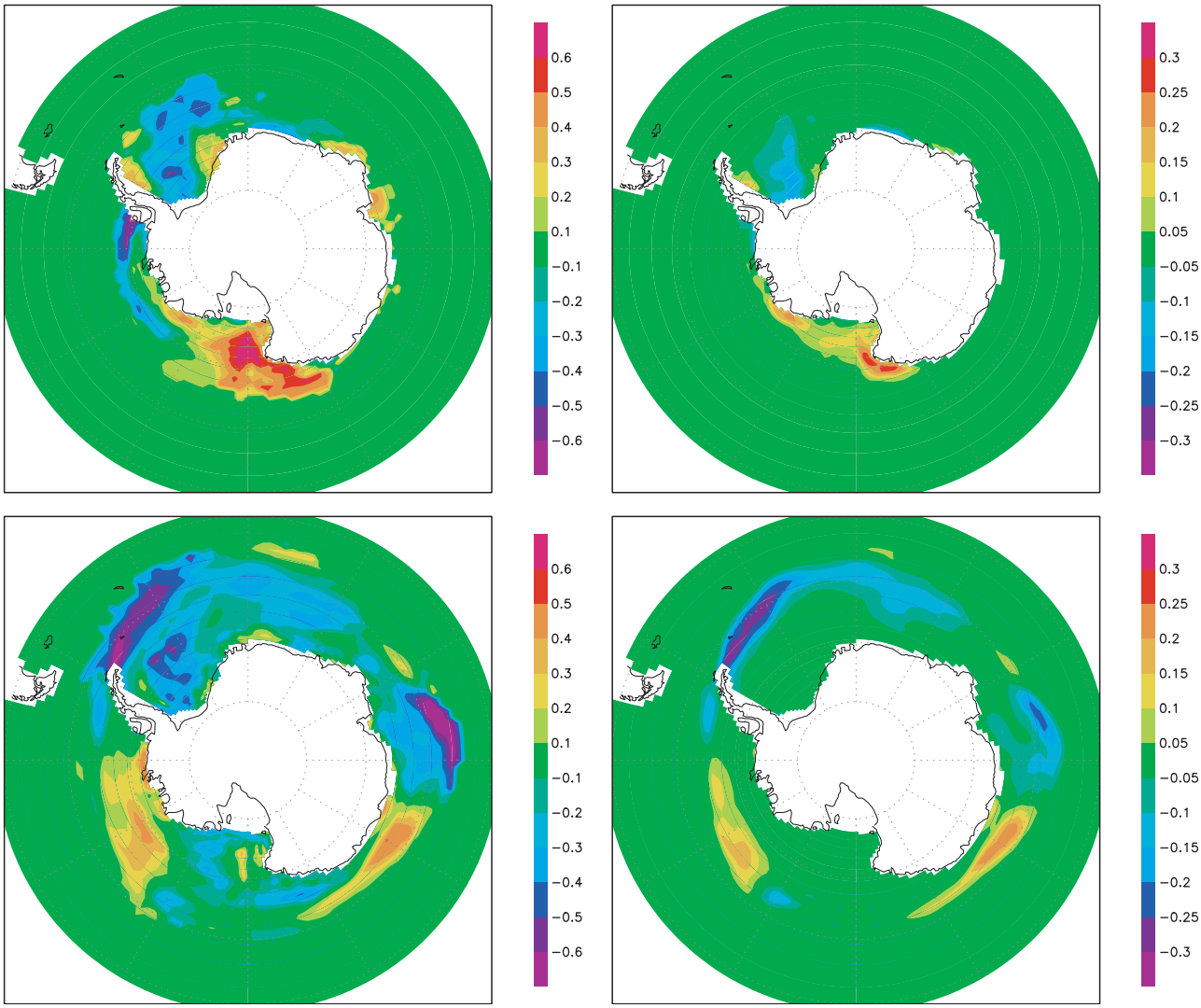

Figure 8. (left) Correlation and (right) regression between the seasonal mean SAM index and the seasonal mean ice concentration for the period 1980–1999 in ORCA2-LIM. (top) January, February, and March. (bottom) July, August, and September.

and Comiso [2002] derived from satellite data. In the western Pacific area between 100°E and 150°E, the signal appears more clear. Both observations and the model (Figures 7 and 8) feature an increase of winter ice concentration near the ice edge. This is due to a large northward sea ice transport in that region for positive phases of SAM (Figure 5, bottom). This can also be clearly seen in the winter ice thickness distribution (not shown), which features an increase offshore and a sharp decrease of ice thickness close to the continent. The response in this region could thus be explained by a mechanism similar to the one described by *Hall and Visbeck* [2002].

[26] The only major disagreement between model and observations occurs in the Indian sector. In this region, the model response shows mainly a decrease in ice concentration during years with positive SAM index, except close to 50°E. In the observations, however, a positive anomaly of ice coverage centered around 50°E covers the majority of the Indian sector, with a decrease in ice concentration only at the boundaries of this sector. Futhermore, in the model the response in the Amundsen Sea appears to be bigger than that close to the Antarctic Peninsula, while it seems to be the opposite in the observations (Table 1).

[27] Thus, our results indicate that the SAM explains only a small fraction of the large-scale variations of sea ice coverage. This is in close agreement with the observational results of *Liu et al.* [2004] and *Kwok and Comiso* [2002]. Nevertheless, some model results are robust and significant, in particular the dipole Weddell Sea–Ross Sea (Table 1).

[28] Note that, except in some regions (like the Ross Sea), the correlation between the SAM index and the ice-covered area is quite low and in particular lower than that of *Hall and Visbeck* [2002], who obtained a correlation of 0.51 between ice coverage and the SAM index. The effect of internal ice stress, which is neglected in the *Hall and Visbeck* [2002] model but considered in LIM, obviously tends to blur the response of the ice pack to anomalies of wind and ocean currents and therefore the close correlation between these fields.

[29] In the evolution of the ice cover in the different sectors of the Southern Ocean described by *Zwally et al.* [2002], a clear influence of the SAM is found only in the Weddell Sea. For instance, the years 1980, 1981, 1991, and 1992 all feature a positive anomaly of sea ice extent in the Weddell Sea while the SAM index is low. The years 1989, 1993, and 1998, which are characterized by a high SAM index, all show an anomalously small ice area in the Weddell Sea. In the other sectors, the influence of the SAM on the ice-covered area is largely overwhelmed by other factors.

[30] In our simulations, there are no substantial salinity (or temperature) changes on the continental shelf associated with the SAM. Furthermore, the response of the mixed layer depth in regions where deep mixing occurs is weak. As a consequence, we can conclude that in our simulation, the SAM does not have a significant impact on the formation of deep waters in the Southern Ocean and, in particular, on the Antarctic Bottom Water (AABW) production.

[31] Although the quality of the forcing data is reduced during the first half of the NCEP-NCAR reanalysis, we have extended our analysis into the period 1960–1979. All the major characteristics of the response of the sea ice-ocean system to SAM are well reproduced for this early period, increasing our confidence in the robustness of our conclusions. For instance, during the period 1960–1979, we still find a decrease of ice extent in the Weddell Sector when the SAM index is positive, along with an increase of ice coverage in the Amundsen sector and an increase of ice between 90°E and 140°E.

4. Conclusions

[32] Using a coupled sea ice-ocean model driven by daily NCEP-NCAR reanalysis data for near-surface air temperatures and winds, and monthly climatologies for humidity, cloudiness, and precipitation, we have confirmed earlier results obtained with CGCMs showing that the Southern Annular Mode (SAM) has a clear and strong impact on the structure of ocean currents over large parts of the water column in the Southern Ocean. At the surface, transport anomalies associated with a positive phase of SAM are directed toward the northwest at high latitudes (south of 45°S) inducing an upwelling that features a maximum around 65°S and a downwelling at about 45°S. Owing to continuity, this is balanced by a southward return flow below 1500 m. Furthermore, the enhanced wind during years with positive SAM index implies a stronger stirring of the water column and a deeper mixed layer during all seasons. The latter and the modification in the intensity of the upwelling, which have both an impact on the availability of nutrients in the upper ocean, might well affect the biological production in the Southern Ocean.

[33] The impact of the SAM on the ocean surface temperature or on the ice-covered area varies strongly for the different regions of the Southern Ocean. Because of a low-pressure anomaly in the Amundsen-Bellingshausen sector during positive SAM years, the Weddell and Bellingshausen Seas are subject to more northerly winds, while the Ross Sea tends to have more southerly winds. This induces a cooling at the surface and an increase in the ice-covered area in the Ross and Amundsen Seas during years with positive SAM index while, at the same time, the SST increases and the ice-covered area decreases in the Weddell Sea. In summary, our results indicate that the main response of the ice concentration to the SAM is a dipole between the Weddell and the Ross Seas with a decrease of ice in the Weddell sector, and an increase in the Amundsen sector and parts of the Pacific sector for years with a positive SAM index. Integrated over the Southern Ocean, these regional differences tend to cancel out, so that signals in the zonally integrated SST and ice concentration are very small.

[34] Those conclusions are statistically significant and in good agreement with observations, and with previous investigations [*Kwok and Comiso*, 2002; *Liu et al.*, 2004]. This suggests that despite the errors in the NCEP-NCAR data set and although the forcing used to drive our simulation does not include interannual variability of cloud cover, precipitation, and relative humidity, we are able to capture, at least qualitatively, the main characteristics of the response of the sea ice-ocean system to the SAM.

[35] Our results also indicate that the recent changes in ice-covered area in the Southern Ocean cannot be attributed to the general increase in the SAM index during the last 20 years. Indeed, an increase in SAM index would imply a less extensive ice cover in the Weddell Sea and a larger area of ice in the Ross Sea. For the Ross Sea this is consistent with observation of the trend performed by *Zwally et al.* [2002], but not for the Weddell Sea. We conclude that the trend observed in the sea ice coverage by *Zwally et al.* [2002] cannot be attributed to the long-term trend of the SAM index. This clearly illustrates that the behavior of the ice cover in the Southern Ocean is a complex phenomena and understanding its evolution needs to take into account all the factors that could affect it [e.g., *Yuan and Martinson*, 1997; *Kwok and Comiso*, 2002; *Van den Broeke*, 2000].

[36] The large regional differences in the response of the Southern Ocean to the SAM may appear strange in the context of an annular mode. Nevertheless, a zonal asymmetry of the temperature pattern can easily be attributed to the non-symmetric land distribution, even with purely zonal winds as argued by *Thompson and Solomon* [2002] to explain the temperature changes over the Antarctic Peninsula. Furthermore, despite its name, the definition of the SAM does not impose that it is strictly an annular phenomenon; the meridional components of the wind appear to play an important role in controlling the ice cover, in particular the low-pressure anomaly over the Bellingshausen-Amundsen Seas during years with positive SAM index. A similar feature occurs in the Northern Hemisphere where the non-zonally symmetric component of the Northern Annular Mode (or NAM, which is closely related to the North Atlantic Oscillation) is responsible for the good correlation between NAM and the ice export through Fram Strait [*Kwok and Rothrock*, 1999; *Hilmer and Jung*, 2000; *Vinje*, 2001]. However, the response of the meridional winds on the NAM appears as a second-order characteristic of the annular mode, not as a first-order one like the change in zonal mean oceanic currents. For instance, the correlation between NAM and the ice export at Fram strait does not hold anymore for long timescales [*Hilmer and Jung*, 2000; *Vinje*, 2001].

[37] **Acknowledgments.** This study is supported by the Federal Science Policy Office (Belgium) (contracts EV/10/7D and EV/10/9A) and the "Action Concertée Incitative Changement Climatique" (Project "Changement Climatique et Cryosphère") from the French Ministry of Research. H. Goosse and T. Fichefet are Research Associates with the Belgian National Fund for Scientific Research. The NCEP-NCAR reanalysis data were provided through the NOAA-CIRES Climate Diagnostics Center, Boulder, Colorado.

References

Beckmann, A., and R. Döscher (1997), A method for improved representation of dense water spreading over topography in geopotential-coordinate models, *J. Phys. Oceanogr.*, *27*, 581–591.

Beckmann, A., and R. Timmermann (2001), Circumpolar influences on the Weddell Sea: Indication of an Antarctic circumpolar coastal wave, *J. Clim.*, *14*, 3785–3792.

Berliand, M. E., and T. G. Strokina (1980), Global distribution of the total amount of clouds (in Russian), report, 71 pp., Hydrometeorological, St. Petersburg, Russia.

Blanke, B., and P. Delecluse (1993), Low frequency variability of the tropical Atlantic Ocean simulated by a general circulation model with mixed layer physics, *J. Phys. Oceanogr.*, *23*, 1363–1388.

Cai, W., and I. G. Watterson (2002), Modes of interannual variability of the Southern Hemisphere circulation simulated by the CSIRO climate model, *J. Clim.*, *15*, 1159–1174.

Connolley, W. M. (1997), Variability in annual mean circulation in southern high latitudes, *Clim. Dyn.*, *13*, 745–756.

Fichefet, T., and M. A. Morales Maqueda (1997), Sensitivity of a global sea ice model to the treatment of ice thermodynamics and dynamics, *J. Geophys. Res.*, *102*(C6), 12,609–12,646.

Fichefet, T., H. Goosse, and M. A. Morales Maqueda (2003a), A hindcast simulation of the Arctic and Antarctic sea-ice variability, 1955−2001, *Polar Res.*, *22*(1), 91–98.

Fichefet, T., B. Tartinville, and H. Goosse (2003b), Antarctic sea ice variability during 1958–1999: A simulation with a global ice-ocean model, *J. Geophys. Res.*, *108*(C3), 3102, doi:10.1029/2001JC001148.

Fischer, H., and P. Lemke (1994), On the required accuracy of atmospheric forcing fields for driving dynamic-thermodynamic sea ice models, in *The Polar Oceans and Their Role in Shaping the Global Environment: The Nansen Centennial Volume*, *Geophys. Monogr. Ser.*, vol. 85, edited by O. M. Johannessen, R. D. Muench, and J. E. Overland, pp. 373–381, AGU, Washington, D. C.

Gent, P. R., and J. C. McWilliams (1990), Isopycnal mixing in ocean circulation models, *J. Phys. Oceanogr.*, *20*, 150–155.

Genthon, C., G. Krinner, and M. Sacchettini (2003), Interannual Antarctic tropospheric circulation and precipitation variability, *Clim. Dyn.*, *21*, 289–307, doi:10.1007/s00382-003-0329-1.

Gong, D., and S. Wang (1999), Definition of Antarctic oscillation index, *Geophys. Res. Lett.*, *26*(4), 459–462.

Goosse, H. (1997), Modelling the large-scale behaviour of the coupled ocean–sea-ice system, Ph.D. thesis, 231 pp., Fac. des Sci. Appl., Univ. Cath. de Louvain, Louvain-la-Neuve, Belgium.

Hall, A., and M. Visbeck (2002), Synchronous variability in the Southern Hemisphere atmosphere, sea ice, and ocean resulting from the Annular Mode, *J. Clim.*, *15*, 3043–3057.

Harder, M., and H. Fischer (1999), Sea ice dynamics in the Weddell Sea simulated with an optimized model, *J. Geophys. Res.*, *104*(C5), 11,151–11,162.

Hibler, W. D., III (1979), A dynamic thermodynamic sea ice model, *J. Phys. Oceanogr.*, *9*, 815–846.

Hibler, W. D., III (1986), Ice dynamics, in *The Geophysics of Sea Ice*, pp. 577–640, Martinus Nijhoff, Dordrecht, Netherlands.

Hilmer, M., and T. Jung (2000), Evidence for recent change in the link between the North Atlantic Oscillation and Arctic sea ice export, *Geophys. Res. Lett.*, *27*, 989–992.

Hines, K. M., D. H. Bromwich, and G. J. Marshall (2000), Artificial surface pressure trends in the NCEP-NCAR reanalysis over the Southern Ocean and Antarctica, *J. Clim.*, *13*, 3940–3952.

Jackett, D. R., and T. J. McDougall (1995), Stabilization of hydrographic data, *J. Atmos. Oceanic Technol.*, *12*, 381–389.

Kalnay, E., et al. (1996), The NCEP/NCAR 40-year reanalysis project, *Bull. Am. Meteorol. Soc.*, *77*, 437–470.

Kidson, J. W. (1999), Principal modes of Southern Hemisphere low-frequency variability obtained from NCEP-NCAR reanalyses, *J. Clim.*, *12*, 2808–2830.

Krahmann, G., and M. Visbeck (2003), Arctic Ocean sea ice response to Northern Annular Mode-like wind forcing, *Geophys. Res. Lett.*, *30*(15), 1793, doi:10.1029/2003GL017354.

Kwok, R., and J. C. Comiso (2002), Southern Ocean climate and sea ice anomalies associated with the Southern Oscillation, *J. Clim.*, *15*, 487–501.

Kwok, R., and D. A. Rothrock (1999), Variability of Fram Strait ice flux and North Atlantic oscillation, *J. Geophys. Res.*, *104*, 5177–5189.

Large, W. G., and S. Pond (1981), Open ocean momentum flux measurements in moderate to strong winds, *J. Phys. Oceanogr.*, *11*, 324–336.

Limpasuvan, V., and D. L. Hartmann (2000), Wave-maintained annular modes of climate variability, *J. Clim.*, *13*, 4414–4429.

Liu, J., J. A. Curry, and D. G. Martinson (2004), Interpretation of recent Antarctic sea ice variability, *Geophys. Res.*, 31, L02205, doi:10.1029/2003GL018732.

Madec, G., P. Delecluse, M. Imbard, and C. Lévy (1999), OPA 8.1 Ocean General Circulation Model reference manual, *Notes du Pôle de Model. 11*, 91 pp., Inst. Pierre-Simon Laplace (IPSL), Jussieu, France.

Marshall, G. J. (2002), Trends in Antarctic geopotential height and temperature: A comparison between radiosonde and NCEP-NCAR reanalysis data, *J. Clim.*, *15*, 659–674.

Merryfield, W. J., G. Holloway, and A. E. Gargett (1999), A global ocean model with double-diffusive mixing, *J. Phys. Oceanogr.*, *29*, 1124–1142.

Mo, K. C. (2000), Relationships between low-frequency variability in the Southern Hemisphere and sea surface temperature anomalies, *J. Clim.*, *13*, 3599–3610.

Proshutinsky, A. Y., and M. A. Johnson (1997), Two circulation regimes of the wind-driven Arctic Ocean, *J. Geophys. Res.*, *102*(12), 12,493–12,514.

Rayner, N. A., D. E. Parker, E. B. Horton, C. K. Folland, L. V. Alexander, D. P. Rowell, E. C. Kent, and A. Kaplan (2003), Global analyses of sea surface temperature, sea ice, and night marine air temperature since the late nineteenth century, *J. Geophys. Res.*, *108*(D14), 4407, doi:10.1029/2002JD002670.

Simmonds, I. (2003), Modes of atmospheric variability over the Southern Ocean, *J. Geophys. Res.*, *108*(C4), 8078, doi:10.1029/2000JC000542.

Stern, H. L., D. A. Rothrock, and R. Kwok (1995), Open water production in Artic sea ice: Satellite measurements and model parameterizations, *J. Geophys. Res.*, *100*(C10), 20,601–20,612.

Stössel, A. (1992), Sensitivity of the Southern Ocean sea-ice simulations to different atmospheric forcing algorithms, *Tellus*, *Ser. A*, *44*, 395–413.

Struraro, G. (2003), A closer look at the climatological discontinuities present in the NCEP/NCAR reanalysis temperature due to the introduction of satellite data, *Clim. Dyn.*, *21*, 309–316, doi:10.1007/s00382-003-0334-4.

Thompson, D. W. J., and S. Solomon (2002), Interpretation of recent Southern Hemisphere climate change, *Science*, *296*, 895–899.

Thompson, D. W. J., and J. M. Wallace (2000), Annular modes in the extratropical circulation: I. Month-to-month variability, *J. Clim.*, *13*, 1000–1016.

Thorndike, A. S., and R. Colony (1982), Sea ice motion in response to geostrophic winds, *J. Geophys. Res.*, *87*(C8), 5845–5852.

Timmermann, R., A. Beckmann, and H. H. Hellmer (2002a), Simulations of ice-ocean dynamics in the Weddell Sea: I. Model description and validation, *J. Geophys. Res.*, *107*(C3), 3024, doi:10.1029/2000JC000741.

Timmermann, R., H. H. Hellmer, and A. Beckmann (2002b), Simulations of ice-ocean dynamics in the Weddell Sea: II. Interannual variability 1985–1993, *J. Geophys. Res.*, *107*(C3), 3025, doi:10.1029/2000JC000742.

Timmermann, R., A. Worby, H. Goosse, and T. Fichefet (2004), Utilizing the ASPeCt sea ice thickness data set to validate a global coupled sea ice–ocean model, *J. Geophys.*, *109*, C07017, doi:10.1029/2003JC002242.

Timmermann, R., H. Goosse, G. Madec, T. Fichefet, C. Ethe, and V. Dulière (2005), On the representation of high latitude processes in the ORCALIM global coupled sea-ice model, *Ocean Modell.*, *8*(1–2), 175–201, doi:10.1016/j.ocemod.2003.12.009.

Trenberth, K. E., J. G. Olson, and W. G. Large (1989), A global ocean wind stress climatology based on the ECMWF analyses, *NCAR/TN-338+STR*, 93 pp., Natl. Cent. for Atmos. Res., Boulder, Colo.

Van den Broeke, M. (2000), The semi-annual oscillation and Antarctic climate: 4. Note on sea ice cover in the Amundsen and Bellingshausen Seas, *Int. J. Climatol.*, *20*, 455–462.

Vinje, T. (2001), Fram Strait ice fluxes and atmospheric circulation: 1950–2000, *J. Clim.*, *14*, 3508–3517.

Watterson, I. G. (2000), Southern midlatitude zonal wind vacillation and its interaction with the ocean in GCM simulations, *J. Clim.*, *13*, 562–578.

Watterson, I. G. (2001), Zonal wind vacillation and its interaction with the ocean: Implication for interannual variability and predictability, *J. Geophys. Res.*, *106*, 23,965–23,975.

Xie, P., and P. A. Arkin (1996), Analyses of global monthly precipitation using gauge observations, satellite estimates and numerical model predictions, *J. Clim.*, *9*, 840–858.

Yuan, X., and D. G. Martinson (1997), Antarctic sea ice area and its global connectivity, *J. Clim.*, *13*, 1697–1717.

Zhang, J., D. A. Rothrock, and M. Steele (2000), Recent changes in Arctic sea ice: The interplay between ice dynamics and thermodynamics, *J Clim.*, *13*, 3099–3114.

Zwally, H. J., J. C. Comiso, C. L. Parkinson, D. J. Cavalieri, and P. Gloersen (2002), Variability of Antarctic sea ice 1979–1998, *J. Geophys. Res.*, *107*(C5), 3041, doi:10.1029/2000JC000733.

T. Fichefet, H. Goosse, and W. Lefebvre, Université Catholique de Louvain, Institut d'Astronomie et de Géophysique Georges Lemaître, Chemin du Cyclotron 2, 1348 Louvain-la-Neuve, Belgium. (lefebvre@astr.ucl.ac.be)

R. Timmermann, Alfred Wegener Institute for Polar and Marine Research, Postfach 12 01 61, 27515 Bremerhaven, Germany.